Laboratory Observation of Transition from Collisional Slow to Collisionless Fast Reconnection

Peiyun Shi,[1,*] Jongsoo Yoo,[1] Hantao Ji,[2,1] Sayak Bose,[1] and Masaaki Yamada[1]
[1]Princeton Plasma Physics Laboratory, Princeton, New Jersey 08543, USA
[2]Department of Astrophysical Sciences, Princeton University, Princeton, New Jersey 08544, USA

(Received 12 September 2025; accepted 20 January 2026; published 24 February 2026)

Temporal transition of an externally driven antiparallel asymmetric magnetic reconnection from collisional slow to collisionless fast regime is observed in a laboratory plasma for the first time. This transition is initiated when the two-fluid Hall effect begins to dominate over collisional effects at the X point, characterized by the ratio of electron-ion collision mean free path to current sheet thickness exceeding unity. Prior to the transition, an enhanced reconnection electric field develops on the low-density side where electrons are heated both ohmically and by large-amplitude lower-hybrid drift waves (LHDW) before collisionality at the X-point drop significantly. These LHDWs generate anomalous resistivity accounting for 30% of the reconnection electric field. The observed time evolution is consistent with the hybrid collisionless-collisional reconnection scenario relevant to onset of asymmetric reconnection in natural plasmas.

DOI: 10.1103/9l36-74my

Introduction—Magnetic reconnection is a fundamental physical process responsible for numerous explosive and energetic phenomena throughout the universe, where magnetic energy is rapidly converted into thermal and kinetic energy of plasmas through the rearrangement of magnetic topology [1,2]. In nature, reconnection occurs in magnetized plasmas across a wide range of collisionality, from the collisional solar chromosphere and planet-forming accretion disks to the highly collisionless solar wind and Earth's magnetosphere [3–5]. Yet, reconnection proceeds much faster than predicted from Sweet-Parker models [6,7] in most cases, a discrepancy often attributed to Hall effects, plasmoid instabilities, or turbulence [8–11]. A magnetic energy build-up phase with slow or no reconnection usually precedes the fast reconnection when stored magnetic energy is released impulsively [12]. This temporal transition has significant implications on the onset of reconnection, a critical yet poorly explored question [13] directly relevant to space weather forecast.

It has been well established that Hall effects enables fast reconnection once the thickness of Sweet-Parker current layer δ_{SP} falls below ion kinetic scales, i.e., ion inertial length d_i for antiparallel reconnection and ion sound speed gyroradius ρ_s for guide-field reconnection [14–17]. A dynamic model for the catastrophic transition from collisional slow to collisionless fast reconnection was proposed by Cassak *et al.* [14] by recognizing an unstable solution emerging from dispersive Hall physics [18,19]. More recently, such transition was identified as a thermodynamic phase transition in fully kinetic simulations of isolated reconnecting current layers [20]. For reconnection with large Lundquist number ($S \gtrsim 10^4$), the transition to fast reconnection can be further facilitated by the formation of plasmoids, which drives rapid thinning of interplasmoid current layers down to ion kinetic scales [21,22].

Transitions in reconnection can also be mediated by various instabilities that are ubiquitously present in currents sheets, whether reconnecting or not, owing to the abundance of free energy sources [23–25]. Among these, the lower-hybrid drift wave (LHDW) is extensively studied as a candidate to generate anomalous resistivity. LHDWs can lead to electron heating, thereby reducing $\delta_{SP} \propto \eta^{1/2}$, where η is the electric resistivity [26–28]. In the nonlinear regime, large-amplitude LHDWs may *indirectly* affect the reconnection rate by modifying the current sheet equilibrium [29]. For instance, LHDWs can result in peaked profiles of current density, which may in turn induces secondary kink or tearing instabilities that facilitate reconnection [30–32]. Recent fully kinetic 3D simulations demonstrate that LHDWs can enhance electron mixing and transport across the separatrices of asymmetric reconnection, potentially altering the evolution of reconnection [33].

In natural plasmas, reconnection is typically highly dynamical or externally driven [34]. The applicability of numerically simulated reconnection transitions remains uncertain, as such transitions are often initiated through imposing large perturbations to an idealized initial current sheet [20,35] that may not necessarily reflect plasma conditions in nature. Observing the temporal evolution of reconnection in space plasmas via *in situ* satellites is also

*Contact author: pshi@pppl.gov

challenging, since the structure crossing time is typically much shorter than the reconnection evolution time scale [25,36]. Remote sensing is more suitable for studying temporal evolution at global scales but is difficult to resolve dynamics at kinetic scales [37]. In this context, laboratory experiments serve as an essentially complementary approach for investigating the dynamics of externally driven time-varying reconnection under controlled and reproducible conditions [38–43].

In this Letter, the time-varying reconnection is generated in a controlled manner by applying an external drive to an initial broad current sheet. The temporal transition of reconnection from collisional slow to collisionless fast regime is initiated when two-fluid effects dominate over collisional effects, i.e., the ratio of the mean free path of electron-ion collisions at the X point to the current sheet thickness exceeds unity. Prior to the transition, plasma on the low-density upstream side becomes collisionless first, which is temporally correlated to a significant decrease of collisionality at the X point. Compared to the collsional high-density upstream, an enhanced E_{rec} is developed at the low-density upstream, consistent with the hybrid collisionless-collisional reconnection scenario [44]. Interestingly, LHDWs driven by pressure gradient are also detected on the low-β_e (electron plasma beta) side. LHDWs heat electrons via anomalous resistivity contributing to the reduction of collisionality on the low-β_e side and decreasing collisionality at the X point, which governs the reconnection rate in weakly collisional plasmas.

Experimental setup and overview—This experiment is conducted in the Magnetic Reconnection Experiment (MRX) device [45]. As shown in Fig. 1(a), deuterium plasmas and reconnection magnetic field are produced by toroidal field (TF) and poloidal field (PF) coils embedded inside the two flux cores. The corresponding current waveforms are displayed in Fig. 1(b). Antiparallel pull reconnection occurs during the ramping down phase of the PF current. The coordinate is defined as follows: R pointing radially outward, Z along the axial reconnecting magnetic field, and Y along the out-of-plane direction of reconnection. The equilibrium field coils provide a static axial magnetic field to maintain reconnection current sheets around $R = 37.5$ cm.

The 2D magnetic probe array consisting of 245 pickup coils measures three-component magnetic field vector $\mathbf{B}(R, Z)$ with spatial resolutions of 2 cm in R and 3 cm in Z. The reconnection current density is given by $\mathbf{J} = \nabla \times \mathbf{B}/\mu_0$, where μ_0 is the vacuum magnetic permeability. The reconnection electric field $E_{\mathrm{rec}} = -(\partial\psi/\partial t)/2\pi R$, where ψ is the in-plane magnetic flux function. Electron temperature T_e and plasma density n_e are measured by triple Langmuir probes. In the MRX plasma parameter regime, probe-induced perturbations are negligible [46], as previously validated against the Thomson scattering diagnostics [47]. The high-frequency

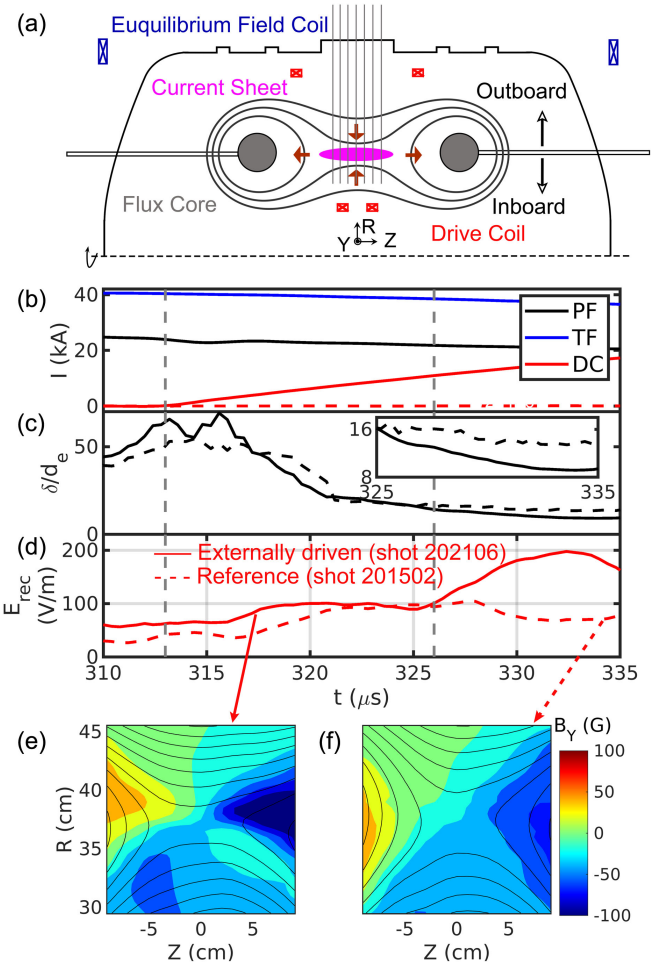

FIG. 1. (a) Schematic representation of the experimental setup for time-varying magnetic reconnection in MRX. Transient behaviors with (solid lines) and without (dashed lines, for reference) external drives: (b) Current of PF (black), TF (blue) and drive coils (DC, red); (c) half-thickness of current sheets δ; inset: enlarged view of δ at later time. (d) Reconnection electric field at the X-point E_{rec}; two vertical gray dashed lines indicate when the external drive starts and when E_{rec} increases significantly. B_Y profiles of the externally driven (e) and reference (f) cases measured at $t = 334$ μs.

fluctuation probe is also employed to measure fluctuation of toroidal electric field δE_Y and plasma density δn_e in the frequency range of $0.1 - 10$ MHz [48].

In contrast to the majority of previous laboratory reconnection experiments, which primarily focused on quasi-steady-state reconnection [9,49,50], this Letter emphasizes transient behaviors of reconnection. A two-step approach is employed to achieve controllable, time-varying reconnection. First, a weakly reconnecting broad current sheet is formed by intentionally reducing the reconnection drive from the PF coil current. Then, a strong external drive is applied via DCs, which generate an additional induction electric field E_Y to further drive reconnection.

Figure 1(d) shows that E_{rec} is nearly doubled reaching 200 V/m, compared to the reference case without external reconnection drive (dashed line). Based on the hybrid Alfvén velocity and reconnecting field defined for asymmetric reconnection [51], the normalized reconnection rate is 0.2 for the externally driven case, larger than 0.1 in reference cases. The reconnection rate in reference cases agrees with predictions from the Sweet-Parker model [49] and is thereby characterized as slow. In contrast, externally driven reconnection proceeds at rates exceeding the predicted Sweet-Parker rate 0.08.

The faster reconnection rate is supported by the formation of Hall magnetic field B_Y shown in Fig. 1(e), suggesting that two-fluid effects dominates [9,52]. For the asymmetric reconnection, B_Y structure deviates from the typical quadrupolar structures, becoming nearly dipolar [50]. For comparison, the B_Y profile of the reference case [see Fig. 1(f)] is generated by the inductive poloidal current in the counter-helicity reconnection [53], with negligible signatures of Hall magnetic field.

The half-thickness of current sheets δ is derived by fitting $B_Z(R)$ to Harris current sheet profiles. Figure 1(c) shows that a thinner current sheet is formed in the externally driven fast reconnection with $\delta/d_e \approx 9$, where d_e is the electron inertial length, smaller than $\delta/d_e \approx 14$ in the reference case at $t = 334$ μs. The additional current sheet thinning is temporally correlated with the increase of E_{rec}. The former δ/d_e ratio is typical for Hall reconnection in MRX, though larger than predictions from numerical simulations [54]. Furthermore, the fast reconnection rate in externally driven case is consistent with the higher magnetic energy conversion rate [55] thanks to both larger E_Y and J_Y indicated by the thinner current sheet.

However, the enhancement of E_{rec} exhibits a significant delay ~13 μs relative to the external reconnection drive, denoted by gray dashed lines in Fig. 1(d). This delay cannot be explained by the typical magnetic diffusion time of an external electromagnetic field (~120 μs). Dynamics processes have to be considered, as previously suggested but not yet explored [56]. This motivates careful examination of the temporal transition from collisional slow to collisionless fast reconnection thanks to the novel reproducible experimental platform. The following Sections are organized by addressing two questions: What is condition for initiating substantial E_{rec} increase and how is this condition achieved? What are responsible dynamic processes for the observed transition?.

Collisionality reduction—To assess the role of collisionality in regulating reconnection rate, we present in Fig. 2(a) the temporal evolution of E_{rec} and the ratio of electron-ion collision mean free path λ_{mfp} to δ at the X point. The significant enhancement of E_{rec} occurs once $\lambda_{\mathrm{mfp}}/\delta$ exceeds unity at $t = 326$ μs, suggesting that low collisionality is a necessary condition for the fast reconnection rate. This is consistent with previous MRX experiments [16,57,58] in

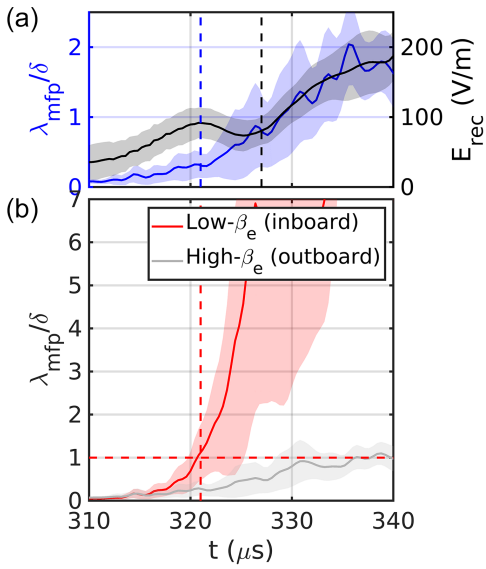

FIG. 2. Temporal evolution of (a) E_{rec} (black), $\lambda_{\mathrm{mfp}}/\delta$ at the X-point (blue), and (b) $\lambda_{\mathrm{mfp}}/\delta$ on the low-β_e inboard side with LHDWs (red) and the high-β_e outboard side without LHDWs (gray). The black dashed line at 326 μs indicates that E_{rec} increases significantly once $\lambda_{\mathrm{mfp}}/\delta$ at the X point passes unity. The red and blue dashed lines both at ~321 μs show collisionality at the X-point decreases more significantly when $\lambda_{\mathrm{mfp}}/\delta$ at the lower density side increases above unity.

that fast reconnection arises when two-fluid effects dominate over collisional effects. During the fully developed Hall reconnection at $t = 340$ μs, the effective resistivity $\eta_{\mathrm{eff}} = E_Y/J_Y \approx 300$ μΩm, larger than the perpendicular Spitzer resistivity of 100 μΩm, suggests dominance of collisionless or kinetic effects for fast reconnection in the collisionless regime. Note that no upstream magnetic flux pileup [59] is observed during the reconnection transition.

It is worth noting that the controlling parameter $\lambda_{\mathrm{mfp}}/\delta$ is effectively equivalent to the more commonly used quantity d_i/δ_{SP} in our experiment regime [16]. Under the condition of ion temperature $T_i = T_e$, and ion beta $\beta_i \approx 1$, $d_i/\delta_{SP} \approx (m_i/4m_e/S)^{1/4}(\lambda_{\mathrm{mfp}}/\delta)^{1/2}$. The first term is estimated to be $1 - 1.5$, indicating that the transition condition $\lambda_{\mathrm{mfp}}/\delta \geq 1$ agrees with $d_i/\delta_{\mathrm{SP}} \geq 1$ within a factor of 2. The collisionality parameter $\lambda_{\mathrm{mfp}}/\delta$ is preferable in experiments as it relies solely on directly measurable quantities whereas d_i/δ_{SP} depends on generalized Sweet-Parker models, specific to realistic boundary and plasma conditions [49].

Distinct from previous results based on quasi-steady-state reconnection, this is the first laboratory observation, to our best knowledge, of the temporal correlation between collisionality and reconnection transition. Interestingly, a similar temporal transition from collisional slow reconnection to collisionless fast Hall reconnection was reported in a fully kinetic simulation of isolated collisional current sheets [20]. In contrast, current sheets are not thermodynamically

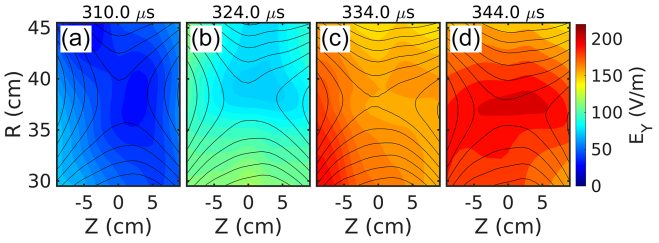

FIG. 3. Toroidal electric field E_Y profiles at different times, t = 310 μs (a), 324 μs (b), 334 μs (c), and 344 μs (d).

isolated in our experiment because electromagnetic energy is continuously fed into current sheets from external coils. This implies that the transition from slow collisional to collisionless fast reconnection may be a universal process of current sheets, dictated by internal plasma dynamics, rather than solely depending on external drives [12].

However, transition to fast reconnection occurs differently between low and high density sides of upstream with a density ratio reaching 5. As shown in Fig. 2(b), the inboard $\lambda_{\rm mfp}/\delta$ on the low-β_e side exceeds unity at $t = 321$ μs (red dashed lines), coinciding with a more rapid reduction of collisionality at the X point, i.e., when the slope of $\lambda_{\rm mfp}/\delta$ at the X point increases significantly [blue dashed line in Fig. 2(a)]. Note that the electron convection time from the inboard upstream to the X point is about 1 μs, within the temporal resolution of measurements. So, no measurably significant delay is expected between red and blue dashed lines, further supporting the causality link between collisionality reduction on the low-β_e side and at the X point. But at the same time, outboard plasmas remain collisional, $\lambda_{\rm mfp}/\delta \approx 0.2$ at $t = 321$ μs mainly due to the higher density, and finally reach unity toward 340 μs. The reconnection with vastly different upstream collisional conditions is in the so-called "hybrid collisional-collisionless" regime, recently demonstrated in laser reconnection experiments by colliding two types of laser-ablated plasmas [44].

Reconnection in the hybrid regime manifests as nonuniform spatial profiles of $E_{\rm rec}$ along R (the inflow direction) at $t = 324$ μs, see Fig. 3(b). $E_{\rm rec}$ reaches 120 V/m on the collisionless inboard side, ∼1.5× that on the collisional outboard side. For reference, no considerable $E_{\rm rec}$ variation along the inflow direction is measured at $t = 310$ μs (during slow collisional reconnection) and $t = 334$ μs (during typical fast collisional reconnection). Eventually, the hybrid collisionless-collisional reconnection evolves into a quasi-steady-state at $t = 344$ μs, as evidenced by the relatively uniform $E_{\rm rec}$ within the narrow current sheet. Therefore, the reduction of inboard collisionality lead to this hybrid regime, serving as an intermediate phase during the transition from slow collisional to fast collisionless reconnection, where large $E_{\rm rec}$ develops on the low-β_e side first and then penetrates into the high-β_e side.

LHDWs and associated electron heating—Now, we investigate the direct plasma response to the external drive

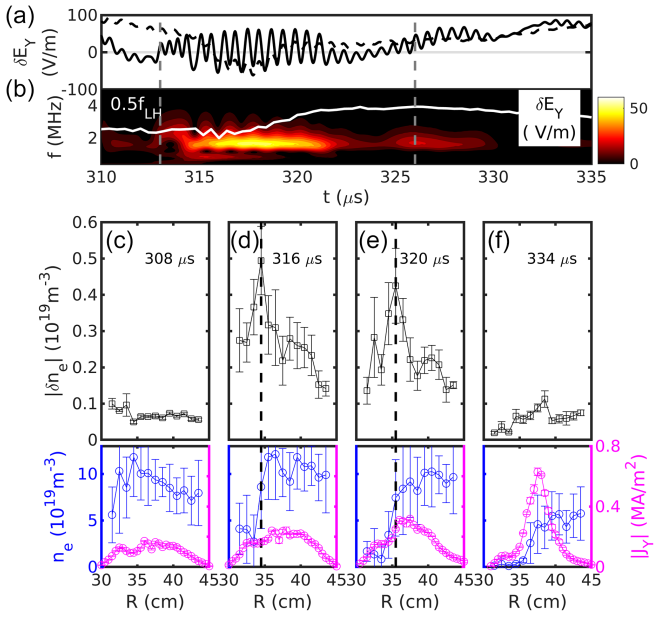

FIG. 4. Top panel: (a) high-frequency fluctuation δE_Y with (black solid line) and without (black dashed line, for reference) external drives; (b) Spectrogram of δE_Y with the overlaying white line denoting half of the lower-hybrid frequency. Same to Fig. 1, two vertical gray dashed lines denote when the external drive starts and when $E_{\rm rec}$ increases significantly. Bottom panel: the spatial profiles of plasma density fluctuation amplitude $|\delta n_e|$ (black squares), plasma density n_e (blue squares), and reconnection current density $|J_Y|$ (magenta circles) and their temporal evolution at $t = 308$ μs (c), 316 μs (d), 320 μs (e), and 334 μs (f).

to elucidate its contribution to the collisionality reduction on the low-β_e side. Figure 4(a) shows that δE_Y emerges shortly after the application of external reconnection drive. For comparison, such fluctuations are absent in the reference case without external reconnection drive. As is shown in Fig. 4(b), the fluctuation frequency is approximately 1.5 MHz ∼ (0.2–0.3)$f_{\rm LH}$, where $f_{\rm LH}$ is the lower-hybrid frequency. The maximum δE_Y amplitude 50 V/m reaches > 50% of $E_{\rm rec}$.

The spatial and temporal evolutions of fluctuation amplitude are presented in Figs. 4(c)–4(f) to help identify the origin of fluctuations. Prior to the application of external reconnection drive, at $t = 308$ μs, the plasma density profile (blue squares) is relatively uniform and fluctuation amplitudes $|\delta n_e| < 0.02 n_e$ are negligible. External E_Y induces larger radial inflow E_Y/B_Z, leading to the formation of a pronounced density gradient at $t = 316$ and 320 μs. As denoted by black dashed lines, the amplitude peaks of δn_e align with the locations of the strongest n_e gradient, instead of the center of current sheets.

The fluctuation amplitude $|\delta n_e|$ decreases as the density gradient diminishes at $t = 334$ μs, even though the reconnection current density $|J_Y|$ continues to increase. This spatial and temporal correlation between fluctuation amplitude and density gradient demonstrates that the observed

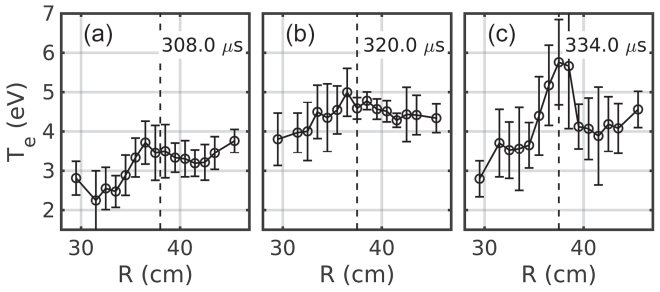

FIG. 5. Spatial profiles of electron temperature T_e at $t = 308$ μs [(a), before LHDWs], 320 μs [(b), during LHDWs], and 334 μs [(c), after LHDWs]. X-point locations are marked by black dashed lines.

fluctuations are electrostatic LHDWs driven by the diamagnetic drift present on the low density side, agreeing well with previous experiments [60]. The measured electron diamagnetic drift velocity 30 km/s is larger than the ion sound speed 15 km/s, a condition favorable for exciting LHDWs [26]. This is also consistent with the fast LHDW growth rate $\sim 0.3\omega_{LH}$, where $\omega_{LH} = 2\pi f_{LH}$, predicted by a local quasilinear LHDW model [61].

The emergence of LHDWs is one direct consequence of the external reconnection drive, which introduces a free energy source of strong density gradient. LHDWs are capable of generating anomalous resistivity to heat electrons, further reducing the electron-ion collisionality [23,27]. Motivated by this, we examine the radial profiles of T_e as a function of time presented in Fig. 5. Before the application of external reconnection drive at $t = 308$ μs when LHDWs are absent, $T_e \approx 2.5$ eV and 3.5 eV on the inboard ($R < 35$ cm) and outboard ($R > 40$ cm) sides, respectively. At $t = 320$ μs, T_e on the inboard side, where LHDWs exist, is increased by $1.5 - 2$ eV, larger than the T_e increase of ~ 1 eV on the outboard side. Because of lower n_e, electron $\beta_e \sim 0.2$ at the inboard LHDW side is much lower than $\beta_e \sim 1$ on the outboard side. The additional T_e increase of $0.5 - 1$ eV at the low-β_e side suggests the localized electron heating associated with LHDWs.

At $t = 334$ μs when LHDW amplitude has significantly attenuated, the T_e profile becomes dominated by reconnection-driven heating around the X point. This is a typical signature of fast reconnection in MRX, which is also supported by the generation of the Hall magnetic field [50]. Notably, T_e on the low-β_e side reduces by ~ 1 eV in the absence of LHDWs, larger than the outboard T_e reduction. This asymmetry of T_e reduction further supports that LHDWs contribute to localized electron heating at $t = 320$ μs.

Discussion—To confirm the contribution of LHDW to electron heating, we calculate the anomalous resistivity term $D_Y = -\langle \delta n_e \delta E_Y \rangle / \langle n_e \rangle = -0.5 \cos\theta (|\delta n_e| / \langle n_e \rangle) |\delta E_Y|$, where $\langle \ldots \rangle$ denotes the temporal average of plasma quantities over several LHDW periods, $\theta = 15°$ is the phase difference between δE_Y and δn_e. The resulting $D_Y \approx 6$ V/m is not negligible, 30% of the Ohmic electric field $\eta_\perp J_Y \approx 20$ V/m. Correspondingly, $\langle \delta E_Y \rangle$ exceeds 50% of mean $E_{\rm rec}$. The anomalous electron heating power density from LHDWs $P_{\rm LHDW} = \langle \delta \mathbf{j} \cdot \delta \mathbf{E} \rangle \sim J_Y D_Y \approx 1.2$ MW/m^3 assuming the electron velocity fluctuation primarily comes from the first order of $\mathbf{E} \times \mathbf{B}$ drift and perpendicular $\langle \delta j_Y \, \delta E_Y \rangle$ dominates based on the local LHDW model with collisions [61]. $P_{\rm LHDW}$ is comparable to the classic Ohmic heating power density ~ 4 MW/m^3, suggesting that both LHDWs and Ohmic heating play important roles in the observed electron heating. For an order of magnitude estimation, the expected T_e increase attributed to LHDWs is $\Delta T_e \sim P_{\rm LHDW} \tau_E / (k_B n_e) \sim 0.3$ eV, qualitatively in agreement with measured T_e increase of $0.5 - 1$ eV, where the electron energy confinement time based on simple random walk model $\tau_E = \tau_{ei} Z_0^2 / \lambda_{\rm mfp}^2 \sim 2$ μs, Z_0 is half the distance between two flux cores and τ_{ei} is the electron-ion collision time.

Since electrostatic LHDWs are primarily localized at the low-β_e side, they are generally not considered to *directly* alter anomalous resistivity at the X point to influence reconnection rate. Nevertheless, LHDWs may influence $E_{\rm rec}$ at the X point *indirectly* via modifying equilibrium profiles of current sheets [32]. In this experiment, the localized electron heating associated with the anomalous resistivity generated by LHDWs contributes to the reduction of collisionality in the low-β_e upstream region. This results in the development of larger $E_{\rm rec}$ in the low-β_e collisionless upstream of hybrid collisionless-collisional reconnection. The heated electrons at the low-β_e side can be transported to the X point via convection or electron mixing [33], further reducing the collisionality at the X point, which initiates the fast kinetic reconnection.

Considering Ohmic heating also contributes significantly to the electron heating at $t = 320$ μs, it remains an open question to which extent LHDWs contributes to the reduction of collisionality at the X point. In addition to the electron heating, LHDWs of large amplitude may influence the electron dynamics and facilitate electron transport to the X point by electron mixing, as demonstrated in one fully kinetic 3D simulation [33].

Given that LHDWs are capable of heating and transporting electrons in quiet current sheets in the absence of active reconnection, LHDWs may play important roles in the onset of reconnection [32]. Laboratory studies of transient reconnection can potentially become essential complementary to recently launched space plasma missions, e.g., Tandem Reconnection and Cusp Electrodynamics Reconnaissance Satellites, primarily targeting temporally and spatially varying reconnection [62,63].

Acknowledgments—This work was supported by NASA Awards No. 80HQTR21T0053, No. NNH20ZDA001N,

No. 80HQTR21T0105, No. 80HQTR21T0060, and No. NNH15AB29I, and DoE Award No. DE-AC0209CH11466.

Data availability—The data that support the findings of this article are openly available [64].

[1] M. Yamada, R. Kulsrud, and H. Ji, Rev. Mod. Phys. **82**, 603 (2010).
[2] H. Ji *et al.*, Space Sci. Rev. **219**, 76 (2023).
[3] L. Ni, B. Kliem, J. Lin, and N. Wu, Astrophys. J. **799**, 79 (2015).
[4] J. Goodman and D. Uzdensky, Astrophys. J. **688**, 555 (2008).
[5] J. L. Burch *et al.*, Science **352**, aaf2939 (2016).
[6] Y.-H. Liu, P. Cassak, X. Li, M. Hesse, S.-C. Lin, and K. Genestreti, Commun. Phys. **5**, 97 (2022).
[7] P. A. Cassak, Y.-H. Liu, and M. A. Shay, J. Plasma Phys. **83**, 715830501 (2017).
[8] J. Birn *et al.*, J. Geophys. Res. **106**, 3715 (2001).
[9] Y. Ren, M. Yamada, S. Gerhardt, H. Ji, R. Kulsrud, and A. Kuritsyn, Phys. Rev. Lett. **95**, 055003 (2005).
[10] A. Bhattacharjee, Y.-M. Huang, H. Yang, and B. Rogers, Phys. Plasmas **16**, 112102 (2009).
[11] A. Lazarian and E. T. Vishniac, Astrophys. J. **517**, 700 (1999).
[12] P. A. Cassak and M. A. Shay, Space Sci. Rev. **172**, 283 (2012).
[13] H. Ji, W. Daughton, J. Jara-Almonte, A. Le, A. Stanier, and J. Yoo, Nat. Rev. Phys. **4**, 263 (2022).
[14] P. A. Cassak, J. F. Drake, M. A. Shay, and B. Eckhardt, Phys. Rev. Lett. **98**, 215001 (2007).
[15] W. Daughton, V. Roytershteyn, B. J. Albright, H. Karimabadi, L. Yin, and K. J. Bowers, Phys. Plasmas **16**, 072117 (2009).
[16] M. Yamada, Y. Ren, H. Ji, J. Breslau, S. Gerhardt, R. Kulsrud, and A. Kuritsyn, Phys. Plasmas **13**, 52119 (2006).
[17] R. G. Kleva, J. F. Drake, and F. L. Waelbroeck, Phys. Plasmas **2**, 23 (1995).
[18] B. N. Rogers, R. E. Denton, J. F. Drake, and M. A. Shay, Phys. Rev. Lett. **87**, 195004 (2001).
[19] P. A. Cassak, M. A. Shay, and J. F. Drake, Phys. Plasmas **17**, 062105 (2010).
[20] J. Jara-Almonte and H. Ji, Phys. Rev. Lett. **127**, 055102 (2021).
[21] W. Daughton, V. Roytershteyn, B. J. Albright, H. Karimabadi, L. Yin, and K. J. Bowers, Phys. Rev. Lett. **103**, 065004 (2009).
[22] A. Stanier, W. Daughton, A. Le, X. Li, and R. Bird, Phys. Plasmas **26**, 072121 (2019).
[23] Y. V. Khotyaintsev, D. B. Graham, C. Norgren, and A. Vaivads, Front. Astron. Space Sci. **6**, 70 (2019).
[24] B. Coppi, G. Laval, and R. Pellat, Phys. Rev. Lett. **16**, 1207 (1966).
[25] T. K. M. Nakamura *et al.*, J. Geophys. Res. **123**, 9150 (2018).
[26] N. A. Krall and P. C. Liewer, Phys. Rev. A **4**, 2094 (1971).
[27] L.-J. Chen *et al.*, Phys. Rev. Lett. **125**, 025103 (2020).
[28] J. Yoo, J. Ng, H. Ji, S. Bose, A. Goodman, A. Alt, L.-J. Chen, P. Shi, and M. Yamada, Phys. Rev. Lett. **132**, 145101 (2024).
[29] G. Lapenta and J. U. Brackbill, Phys. Plasmas **9**, 1544 (2002).
[30] P. Ricci, J. U. Brackbill, W. Daughton, and G. Lapenta, Phys. Plasmas **11**, 4489 (2004).
[31] R. Horiuchi and T. Sato, Phys. Plasmas **6**, 4565 (1999).
[32] W. Daughton, G. Lapenta, and P. Ricci, Phys. Rev. Lett. **93**, 105004 (2004).
[33] A. Le, W. Daughton, L.-J. Chen, and J. Egedal, Geophys. Res. Lett. **44**, 2096 (2017).
[34] E. G. Zweibel and M. Yamada, Annu. Rev. Astron. Astrophys. **47**, 291 (2009).
[35] W. Daughton, J. Scudder, and H. Karimabadi, Phys. Plasmas **13**, 072101 (2006).
[36] K. J. Genestreti, P. A. Cassak, A. Varsani, J. L. Burch, R. Nakamura, and S. Wang, Geophys. Res. Lett. **45**, 2886 (2018).
[37] G. Chisham *et al.*, Rev. Geophys. **46**, RG1004 (2008).
[38] N. Katz, J. Egedal, W. Fox, A. Le, J. Bonde, and A. Vrublevskis, Phys. Rev. Lett. **104**, 255004 (2010).
[39] J. Jara-Almonte, H. Ji, M. Yamada, J. Yoo, and W. Fox, Phys. Rev. Lett. **117**, 095001 (2016).
[40] P. Shi, P. Srivastav, M. H. Barbhuiya, P. A. Cassak, E. E. Scime, and M. Swisdak, Phys. Rev. Lett. **128**, 025002 (2022).
[41] W. Gekelman, T. D. Haas, W. Daughton, B. V. Compernolle, T. Intrator, and S. Vincena, Phys. Rev. Lett. **116**, 235101 (2016).
[42] S. Dorfman, H. Ji, M. Yamada, J. Yoo, E. Lawrence, C. Myers, and T. D. Tharp, Phys. Plasmas **21**, 012109 (2014).
[43] Y. Liu, P. Shi, X. Zhang, J. Lei, and W. Ding, Rev. Sci. Instrum. **92**, 71101 (2021).
[44] Z. Zhao *et al.*, Commun. Phys. **5**, 247 (2022).
[45] M. Yamada, H. Ji, S. Hsu, T. Carter, R. Kulsrud, N. Bretz, F. Jobes, Y. Ono, and F. Perkins, Phys. Plasmas **4**, 1936 (1997).
[46] F. F. Chen, Langmuir probe diagnostics, in *Proceedings of the Mini-Course on Plasma Diagnostics (IEEE-ICOPS'03), Jeju, Korea*, (Institute of Electrical and Electronics Engineers, Jeju, Korea, 2003).
[47] M. Kaloyan, S. Ghazaryan, S. P. Tripathi, W. Gekelman, M. J. Valle, B. Seo, and C. Niemann, Instruments **6**, 17 (2022).
[48] Y. Hu, J. Yoo, H. Ji, A. Goodman, and X. Wu, Rev. Sci. Instrum. **92**, 033534 (2021).
[49] H. Ji, M. Yamada, S. Hsu, and R. Kulsrud, Phys. Rev. Lett. **80**, 3256 (1998).
[50] J. Yoo, B. Na, J. Jara-Almonte, M. Yamada, H. Ji, V. Roytershteyn, M. R. Argall, W. Fox, and L.-J. Chen, J. Geophys. Res. **122**, 9264 (2017).
[51] P. A. Cassak and M. A. Shay, Phys. Plasmas **14**, 102114 (2007).
[52] F. Yang *et al.*, Geophys. Res. Lett. **52**, e2024GL114151 (2025).
[53] M. Inomoto, S. P. Gerhardt, M. Yamada, H. Ji, E. Belova, A. Kuritsyn, and Y. Ren, Phys. Rev. Lett. **97**, 135002 (2006).
[54] H. Ji, Y. Ren, M. Yamada, S. Dorfman, W. Daughton, and S. P. Gerhardt, Geophys. Res. Lett. **35**, L13106 (2008).

[55] M. Yamada, J. Yoo, J. Jara-Almonte, H. Ji, R. M. Kulsrud, and C. E. Myers, Nat. Commun. **5**, 4774 (2014).
[56] J. Xie, P. Shi, H. Ji, J. Jara-Almonte, J. Yoo, Y. Okunishi, S. Dorfman, and M. Yamada, Phys. Plasmas **31**, 022108 (2024).
[57] A. Kuritsyn, H. Ji, S. P. Gerhardt, Y. Ren, and M. Yamada, Geophys. Res. Lett. **34**, L16106 (2007).
[58] F. Trintchouk, M. Yamada, H. Ji, R. M. Kulsrud, and T. A. Carter, Phys. Plasmas **10**, 319 (2003).
[59] T. P. Intrator, X. Sun, G. Lapenta, L. Dorf, and I. Furno, Nat. Phys. **5**, 521 (2009).
[60] T. A. Carter, H. Ji, F. Trintchouk, M. Yamada, and R. M. Kulsrud, Phys. Rev. Lett. **88**, 015001 (2001).
[61] J. Yoo, Y. Hu, J.-Y. Ji, H. Ji, M. Yamada, A. Goodman, K. Bergstedt, W. Fox, and A. Alt, Phys. Plasmas **29**, 022109 (2022).
[62] C. Kletzing, The Tandem Reconnection And Cusp Electrodynamics Reconnaissance Satellites (TRACERS) Mission, in *AGU Fall Meeting Abstracts*, Vol. 2019 (2019), pp. A41U–2687.
[63] D. M. Miles *et al.*, Space Sci. Rev. **221**, 61 (2025).
[64] P. Shi, Version 1, Name of Repository—Princeton Data Commons (2026), 10.34770/fk8v-f575.